

1 **A non-destructive approach for measuring rice panicle-level photosynthetic responses**
2 **using 3D-image reconstruction**

3 Jaspinder Singh Dharni*¹, Balpreet Kaur Dhatt*¹, Puneet Paul*¹, Tian Gao², Tala Awada³, Paul
4 Staswick¹, Jason Hupp⁴, Hongfeng Yu², Harkamal Walia^{1,†}

5
6 ¹Department of Agronomy and Horticulture, University of Nebraska-Lincoln, NE 68583, USA

7 ²Department of Computer Science and Engineering, University of Nebraska-Lincoln, NE 68588,
8 USA

9 ³School of Natural Resources, University of Nebraska-Lincoln, Lincoln, NE 68583, USA

10 ⁴LI-COR Inc. 4647 Superior Street, Lincoln, NE 68505, USA

11 * These authors contributed equally to this work.

12 † Author for correspondence: Harkamal Walia (ORCID ID: 0000-0002-9712-5824)

13 *Tel:* (402) 472-1162, *Email:* hwalia2@unl.edu

14 ORCID IDs and Twitter accounts

15 JSD: 0000-0003-1780-2045 (@SJaspinder1)

16 BKD: 0000-0002-3577-962X (@dhattbalpreet)

17 PP: 0000-0001-8220-8021 (@paulpuneet)

18 TG: 0000-0003-4075-4125

19 PS: 0000-0003-2798-0275

20 Total word count (excluding summary, references, conclusion, acknowledgements, and legends):

21 6159

22 Summary: 209, Introduction: 949, Materials and Methods: 1887, Results: 2220, Discussion:

23 1103, Conclusion: 83, Acknowledgements: 48, No. of figures: 7, No. of Supporting Information

24 files: 7 (Fig. S1-S7).

25 **Summary**

26 Our understanding of the physiological response of rice inflorescence (panicle) to environmental
27 stresses is limited by the challenge of accurately determining panicle photosynthetic parameters
28 and their impact on grain yield. This is primarily due to lack of a suitable gas exchange
29 methodology for panicles, as well as non-destructive methods to accurately determine panicle
30 surface area. To address these challenges, we have developed a custom panicle gas exchange
31 cylinder compatible with the LiCor 6800 Infra-red Gas Analyzer. Accurate surface area
32 measurements were determined with a 3D panicle imaging platform to normalize the panicle-level
33 photosynthetic measurements. We observed differential responses in both panicle and flag leaf for
34 two temperate Japonica rice genotypes (accessions, TEJ-1 and TEJ-2) exposed to heat stress during
35 early grain filling. There was a notable divergence in relative photosynthetic contribution of flag
36 leaf and panicles for the genotype tolerant to heat stress (TEJ-2) compared to the less tolerant
37 accession. The novelty of this approach is that it is non-destructive and more accurately determines
38 panicle area and photosynthetic parameters, enabling researchers to monitor temporal changes in
39 panicle physiology during the reproductive development. The method is useful for panicle-level
40 measurements under diverse environmental stresses, and for evaluating genotypic variation for
41 panicle physiology and architecture in other cereals with compact inflorescences.

42 **Key words:** rice, panicle, carbon assimilation, transpiration, imaging, heat stress, photosynthesis

43

44

45

46

47

48

49

50

51

52

53 Introduction

54 Rice (*Oryza sativa*) is a crucial crop for global food security. However, rice production is
55 susceptible to heat stress (HS) (Dhatt *et al.*, 2019; Khush, 2005; Khush & Jena, 2009; Muthayya
56 *et al.*, 2014; Prasad *et al.*, 2017; Peng *et al.*, 2004; Moore *et al.*, 2021). Rice reproductive
57 development is considered the most heat sensitive stage (Ali *et al.*, 2019; Arshad *et al.*, 2017; S.
58 V.K. Jagadish *et al.*, 2007; S. V.Krishna Jagadish, 2020; Paul *et al.*, 2020a). Even a short duration
59 of heat stress during early grain development affects mature grain size and weight parameters
60 (Chen *et al.*, 2016; Folsom *et al.*, 2014; Kadan *et al.*, 2008; Lisle *et al.*, 2000; Sreenivasulu *et al.*,
61 2015). During the reproductive stage, rice grain is the primary sink organ whose normal
62 development depends upon the accumulation and utilization of photoassimilates from leaves
63 (Zhang *et al.*, 2018; Abdelrahman *et al.*, 2020). Recent studies suggest that in addition to being a
64 temporary sink, panicles also contribute to the grain photoassimilate pool and consequently to
65 grain yield (Kong *et al.*, 2016; Tambussi *et al.*, 2021; Vicente *et al.*, 2018a; Chang *et al.*, 2020).

66
67 A better understanding of source-sink dynamics in the context of photosynthetic responses and
68 grain filling is needed for predicting how grain yield parameters are affected by temperature (Gao
69 *et al.*, 2021; Lubis *et al.*, 2003; Wang *et al.*, 2020). In absence of further improvement in rice heat
70 resilience, it is estimated that for every 1°C increase in temperature, there will be ~ 3.2% decline
71 in yield (Zhao *et al.*, 2017). From a mechanistic perspective much of that impact could be due to
72 temperature sensitivity of the plant's photosynthetic capacity and the cellular processes of
73 developing seed. Heat stress impacts photosynthesis in multiple ways, including increasing
74 membrane permeability in leaves, damaging sub-cellular membranes such as thylakoid
75 membranes, thus impeding light harvesting, electron transport rates and ATP generation (Schrader
76 *et al.*, 2004; Prasad *et al.*, 2008; Djanaguiraman *et al.*, 2013; Pokharel *et al.*, 2020). Under HS the
77 primary carbon-fixing enzyme, rubisco, is also more active as an oxygenase leading to the
78 production of 2-phosphoglycolate, which is eliminated through the photorespiratory pathway
79 resulting in partial loss of previously fixed carbon (Walker *et al.*, 2016; Moore *et al.*, 2021).
80 Altogether, the reduced photosynthetic efficiency and increased respiration-photorespiration rates
81 due to HS alter the dynamics between source and sink organs, leading to yield decline (Prasad *et*
82 *al.*; Ferguson *et al.*, 2021).

83

84 The capacity of primary source tissue to mobilize photoassimilates and the ability of sink tissue
85 (grain) to accumulate the transported sugars determines the extent of grain filling (Zhang *et al.*,
86 2018; Abdelrahman *et al.*, 2020). A significant proportion of the assimilates accumulating in the
87 grains are derived from the upper canopy (Austin *et al.*, 1977; Bidinger *et al.*, 1977.; Inoue *et al.*,
88 2004). One estimate suggests that the youngest three leaves may contribute over 50% of the
89 assimilates into the rice grain filling pool (Li *et al.*, 1998). While foliar tissue is the primary source
90 of photoassimilates, non-foliar tissue such as developing rice panicles are also photosynthetically
91 active and contribute towards photoassimilate accumulation in grains (Tambussi *et al.*, 2007;
92 Maydup *et al.*, 2012). There is limited evidence supporting the role of green inflorescence tissues
93 as contributor to carbon assimilation (A_{gross}) equivalent to ~30% of the flag leaf (Grundbacher *et*
94 *al.*, 1963; Imaizumi *et al.*, 1990). However, effect of HS on the net photosynthetic contributions
95 by non-foliar organs and the dynamic relationship between foliar and non-foliar organs is not
96 explored in rice. The extent of genotypic variation for these responses is also unknown.

97
98 The temporal evaluation of foliar photosynthetic parameters on a per unit area basis can be
99 accomplished non-destructively using well-established protocols. Instrumentation for these
100 experiments is designed for laminar leaf surfaces for which precise surface areas can be
101 determined. However, measurement of non-laminar organs (inflorescence/panicle) with their
102 intricate and complex architectures is challenging (Simkin *et al.*, 2020). This issue has been
103 partially addressed recently (Chang *et al.*, 2020), where panicle area was computed for evaluating
104 non-foliar photosynthetic parameters. However, this approach limits evaluation of temporal
105 responses due to the destructive sampling of panicles for each measurement. Recent advances in
106 image-based plant phenotyping have enabled the development of a 3D-panicle imaging platform
107 (*PI-Plat*) for high-resolution, temporal assessment of vegetative and inflorescence-related traits in
108 a non-destructive and precise manner (Sandhu *et al.*, 2019; Zhu *et al.*, 2021a; Zhu *et al.*, 2021b).
109 Digital traits derived from 3D reconstructed panicles are more sensitive and accurate than results
110 from 2D images (Sandhu *et al.*, 2019). Thus, the non-destructive estimation of panicle size
111 parameters in rice using 3D-imaging platforms can be used to establish surface area normalized
112 panicle photosynthetic assessments.

113

114 We combined panicle surface area measurements with a customized gas exchange cylinder that
115 allowed unrestricted enclosure of panicles, thus overcoming a major limitation of shading as
116 reported in other studies (Maydup *et al.*, 2012; Sanchez-Bragado *et al.*, 2016; Chang *et al.*, 2020).
117 Measuring flag leaf and panicle photosynthetic parameters concurrently enabled us to identify
118 relationships between foliar and non-foliar tissue gas exchange rates under control and HS
119 conditions. This novel approach was able to identify changes in source-sink dynamics in response
120 to HS, as well as differential response of two temperate japonica rice accessions that were
121 previously known to differ in their sensitivity to HS during grain development (GSOR Ids: 301110,
122 TEJ-1 and 301195, TEJ-2) (Paul *et al.*, 2020). Our results establish a viable method for more
123 precise temporal evaluation of source-sink relationships during reproductive development, in
124 response to HS, for the study of genetic diversity in photosynthetic strategies among rice
125 accessions. Although we specifically examined HS response, the method should also be useful
126 under other stress conditions as well.

127

128 **Materials and Methods**

129 *Plant material and growth conditions*

130 Two temperate japonica rice genotypes, GSOR Ids: 301110 (TEJ-1) and 301195 (TEJ-2), were
131 selected based on their heat stress (HS) response (Paul *et al.*, 2020). Mature seeds from the two
132 accessions were dehusked using a Kett TR-130, sterilized with water and bleach (40%, v/v), and
133 rinsed with sterile water. The seeds were germinated in the dark on half-strength Murashige and
134 Skoog media. After five days, germinated seedlings were transplanted to soil in 4-inch square pots,
135 and plants were grown under control greenhouse conditions: 16 h light and 8 h dark at $28\pm 1^\circ\text{C}$ and
136 $23\pm 1^\circ\text{C}$, respectively. Relative humidity ranged from 55-60% throughout the experiments.

137

138 *Heat stress treatments*

139 A set of plants was used to do the PI-Plat imaging and provide photosynthetic measurements using
140 the LI-6800. Plants were grown under control conditions until flowering. Once flowering initiated,
141 the primary panicle was carefully examined. Since the primary panicle is the first one to flower,
142 we focused on measuring its photosynthetic parameters along with flag leaf for experimental
143 accuracy. Upon ~50% completion of primary panicle flowering, a set of plants was either kept
144 under control conditions (16 h light and 8 h dark at $28\pm 1^\circ\text{C}$ and $23\pm 1^\circ\text{C}$) or moved to greenhouse

145 set-up for a moderate heat stress (HS) treatment (16 h light and 8 h dark at $36\pm 1^\circ\text{C}$ and $32\pm 1^\circ\text{C}$).
146 We used these plants for primary panicle imaging and photosynthetic measurements at 4 and 10
147 days after fertilization (DAF) under control and HS conditions (Fig. 4 and S1).

148
149 Another set of plants was used for measuring the mature seed yield-related traits. Florets were
150 marked at the time of fertilization to track developing seeds. 1 DAF, plants were kept in either
151 control conditions (16 h light and 8 h dark at $28\pm 1^\circ\text{C}$ and $23\pm 1^\circ\text{C}$) or moved to greenhouse setup
152 for a moderate HS treatment (16 h light and 8 h dark at $36\pm 1^\circ\text{C}$ and $32\pm 1^\circ\text{C}$). The plants were
153 subjected to HS treatment for either 2 to 4 DAF (HS-I), or 2 to 10 DAF (HS-II). Afterward, plants
154 were moved back to control temperature conditions and harvested at physiological maturity to
155 analyze mature grain yield-related parameters (Fig. S4a).

156

157 *Panicle imaging and downstream analysis*

158 *Image Acquisition*

159 We utilized the Panicle Imaging Platform (PI-Plat) to capture rice panicle images (Gao et al., 2021;
160 Sandhu et al., 2019). Briefly, PI-Plat is comprised of customized wooden chamber (Fig. S1) with
161 a circular wooden board, parallel to the floor, having an aperture at its center. Plants marked for
162 imaging were brought into the chamber, and the primary panicle of the plant was passed through
163 the aperture. A rotary apparatus hosting two Sony $\alpha 6500$ cameras and LED lights (ESDDI PLV-
164 380, 15 watts, 500 LM, 5600 K) rotated 360° around the panicle. With the built-in time-lapse
165 application, each camera took an image per second for one minute. The two cameras generate 120
166 images for one panicle with a resolution of 6000×4000 pixels. Color checkerboards were placed
167 on the chamber and table to facilitate camera parameters recovery and correspondence detection
168 in paired images (Fuhrmann *et al.*, 2014).

169

170 *3D Point Cloud Reconstruction*

171 Captured panicle images were pre-processed to remove the background. To achieve this, images
172 were first converted from the red, green, and blue (RGB) color space into the hue, saturation, and
173 value (HSV) color space. Then, we implemented color thresholding using the MATLAB
174 application "colorthresholder". Pixels were removed if their corresponding hue, saturation, and
175 value were not in the range of 0–1, 0–1, and 0.15–1, respectively. Next, the pre-processed images

176 were used for 3D reconstruction. To reconstruct the Panicle's point cloud, we implemented the
177 Multi-View Environment (MVE) pipeline (Fuhrmann *et al.*, 2014). The MVE pipeline detected
178 and matched the image features in the pre-processed images. A parse point cloud was generated
179 based on matched image features. The parameters of cameras, including position and orientation,
180 were also extracted in this process. Afterward, a dense point cloud was generated by calculating
181 the depth information for each pixel in each image using the cameras' parameters. Finally, floating
182 scale surface reconstruction (FSSR) (Fuhrmann & Goesele, 2014) was implemented to denoise the
183 dense point cloud.

184 The reconstructed point clouds of the MVE pipeline included all the objects in the scene. We
185 removed uninteresting objects from the original point cloud by implementing color thresholding
186 and connected component labeling to calculate the panicle features in the next section. First, we
187 segmented the panicle's point cloud cluster by computing the Visible Atmospherically Resistant
188 Index (VARI) (Gitelson *et al.*, 2002) for each point in the point cloud. Equation (1) shows the
189 formula of VARI, where R, G, and B mean the corresponding intensity of a point in the RGB color
190 space.

$$191 \quad \text{VARI} = \frac{G - R}{G + R - B} \quad (1)$$

192

193 The cluster containing the maximum number of points whose VARI > 0.1 is considered as the
194 panicle. Then, we filtered out uninteresting points in the cluster, for instance, plant labels. A
195 representative image of the final point cloud that includes only the panicle is shown in Fig. 1a.

196

197 *Trait Extraction*

198 In this study, each point cloud was voxelized for volume quantification (Cohen-Or & Kaufman,
199 1995). The corresponding resulting volume was then used to extract traits of interest, for instance,
200 voxel count and color intensity (Sandhu *et al.* 2019). Also, we calculated the projected surface
201 area. The projected surface area was used to estimate the surface area of the panicle. We first
202 calculated point cloud's main directions using principal component analysis (PCA) to compute the
203 projected surface area. There were three main directions in a given 3D point cloud. We built 3D
204 coordinate system using the first main direction as Z-axis and the other two directions as the X-
205 and Y-axes. The origin of the system was defined as the lowest point of the point cloud, which

206 was located at the bottom of the panicle. Then, we generated a plane using Y-axis as the norm.
207 After projecting the point cloud of the panicle onto the plane, we calculated the projected surface
208 area as the area of the region enclosed by the boundary of the projected 2D points (Fig. 1b).
209 Afterward, we rotated the plane around the Z-axis and calculated the projected surface area every
210 5 degrees. In total, we captured 36 projected surface areas. We finally extracted the maximal
211 projected area, the minimal projected area, and the averaged projected area from these results. We
212 used averaged projected area for final analysis and normalization of panicle's photosynthetic
213 parameters. We also computed the projection area when the plane was perpendicular to the X-axis
214 and Y-axis. Apart from computing the image derived traits (projected surface area, voxel counts,
215 and color intensity) from an entire panicle, we also examined additional traits extracted from local
216 regions of the panicles. We divided the 3D panicle into 10 equal sections along the Z-axis to
217 generate 10 slices. For each slice, we analyzed the corresponding traits (i.e., point count and point
218 color). The analysis of sliced 3D traits enabled us to examine spatial and temporal variation in the
219 development of grains on a particular panicle.

220

221 *Leaf and Panicle photosynthetic measurements*

222 Two LI-6800 (LI-COR) devices were used in parallel to measure leaf and panicle-based gas
223 exchange variables (Fig. 4). All photosynthetic measurements were recorded between 1100-1400
224 hours. For photosynthetic measurements, the environmental conditions were set as: Relative
225 humidity chamber at 50%, flow rate at $700 \mu\text{mol s}^{-1}$, chamber pressure at 0.05 kPa, light intensity
226 at $800 \mu\text{mol m}^{-2}\text{s}^{-1}$, and reference CO_2 at $400 \mu\text{mol mol}^{-1}$. LI-6800 warm-up tests were conducted
227 every time before the actual measurements to control the error rates. To maintain the incident
228 radiation intensity between $800\text{-}900 \mu\text{mol m}^{-2} \text{s}^{-1}$ in the greenhouse setting, two adjustable
229 additional LED lights (Vipar Spectra; Model: V300) were used as a source of diffused light. These
230 LED lights included IR (Infrared) LEDs that looked dim/invisible and operated at input voltage
231 120V and 60Hz frequency. Plants were acclimatized to the artificial light for 15-20 minutes before
232 recording the photosynthetic measurements. One of the LI-6800s was used for measuring gas
233 exchange from the flag leaf, while the other one with an equipped cylinder chamber was used to
234 measure panicle-based photosynthesis on the same plant (Fig. 4). The sensor head of LI-6800 was
235 fitted onto the customized cylindrical chamber having a height and radius of 25.4 and 2.8 cm,
236 respectively, to measure panicle-level incidence light. The bottom end of the cylinder was

237 equipped with a rubber stopper with a small hole facilitating insertion of the panicle stalk. The
238 customized chamber was further sealed with modeling clay each time after inserting the panicle to
239 prevent air leakage. Leaf level measurements were taken after inserting a specified region of a flag
240 leaf into the LI-6800 head; however, panicle-based measurements encompassed the whole panicle.
241 Further, to verify the functioning of our customized chamber, we measured the photosynthetic
242 parameters of young leaves using both traditional chamber and customized chamber (Fig. S6).
243 Unlike panicle, we were not able to completely control the leakage by using customized chamber
244 for taking leaf level photosynthetic measurements. Although no significant differences were
245 observed between values derived from traditional chamber and customized chamber for the leaf
246 measurements, the values from customized chamber were slightly higher due to minimal leakage
247 (Fig. S6). The gas exchange readings from flag leaf and panicle of a particular plant stabilized after
248 10-15 minutes, after which the setup was used for measuring the next plant. Since LI-6800
249 measured gas exchange variables were based on per unit area, the surface area of panicles was
250 determined by panicle imaging and then used to normalize the data. The parameters considered
251 for photosynthetic measurements were A_{leaf} (leaf carbon assimilation), $g_{sw_{leaf}}$ (leaf stomatal
252 conductance), E_{leaf} (apparent leaf transpiration rate), VPD_{leaf} (vapor pressure deficit inside leaf
253 chamber), $A_{panicle}$ (panicle carbon assimilation), and $E_{panicle}$ (apparent panicle transpiration rate).
254 The term “apparent” transpiration rate was used in this study to distinguish it from the transpiration
255 rate occurring under natural unenclosed conditions. Furthermore, we calculated water use
256 efficiency (WUE) of leaf (WUE_{leaf}) and panicle ($WUE_{panicle}$) separately by dividing respective
257 carbon assimilation rate (A) with their apparent transpiration rate (E).

258 *Correlation analysis*

259 We considered data from 3 digital (green pixels proportion, voxel count, and projected panicle
260 area) and four physiological ($A_{panicle}$, $E_{panicle}$, A_{leaf} , E_{leaf}) traits for computing a pairwise Pearson
261 correlation (PCC). Each trait consisted of an observation from three biological replicates under
262 control and HS from accessions TEJ-1 and TEJ-2. PCC between a pair of traits was computed in
263 RStudio v.1.2.5033 platform. We computed PCC separately for TEJ-1 and TEJ-2 at 10 DAF under
264 HS, as the two accessions had a contrasting performance at this time point under HS. The
265 correlation matrix plot and significance level was generated using the 'chart.Correlation' function
266 incorporated in the 'PerformanceAnalytics' package.

267

268 *Mature seed analysis*

269 To assess effect of moderate HS on mature seeds, we first evaluated only florets marked at the
270 time of fertilization (Dhatt *et al.*, 2021). For this, we scored the total number of fully developed
271 and unfilled or completely sterile seeds to calculate percentage fertility. The dehusked mature
272 seeds were used to measure (i) morphometric parameter (length, width), (ii) single grain weight,
273 (iii) percent fertility. Morphometric analysis was performed on 350–1000 marked seeds from 20–
274 40 plants using *SeedExtractor* (Zhu *et al.*, 2021a). Secondly, to have insights into yield-related
275 parameters at a whole plant level, we evaluated all the seeds for percentage fertility and total seed
276 weight per plant.

277

278 **Results**

279 *Heat stress induces differential morphological responses in panicles*

280 The purpose of this study was to establish whether multi-view images captured by using PI-Plat
281 could be combined with a novel method for whole panicle gas exchange measurements to follow
282 photosynthetic dynamics during reproductive development. We imposed a moderate HS for 4 or
283 10 days beginning one day after fertilization (DAF) and measured the photosynthetic response of
284 both foliar and panicle tissue under control (28/23°C; day/night) and HS (36/32°C; day/night). Two
285 rice lines (TEJ-1 and TEJ-2) genetically diverse in their response to HS were compared. From
286 captured images from multiple angles 3D point clouds of panicles were reconstructed to extract
287 the digital traits of a panicle (Fig. 1). The derived digital traits included, projected panicle area
288 (PPA), voxel count (VC), and color intensity (red and green pixels) representing the panicle's area,
289 volume, and green/red pixel proportion, respectively (Gao *et al.*, 2021; Sandhu *et al.*, 2019). We
290 first used the digital traits to examine whether they could distinguish temporal differences in
291 inflorescence architecture due to HS, and then whether the response differed between TEJ-1 and
292 TEJ-2 (Fig. 2). In TEJ-1, PPA exhibited an increase from 4 to 10 DAF under control conditions,
293 while no significant change was observed under HS (Fig. 2a). An increase in PPA was also
294 observed in TEJ-2 from 4 to 10 DAF under control conditions. However, unlike TEJ-1, TEJ-2
295 exhibited an increase in PPA from 4 to 10 DAF under HS (Fig. 2a). VC also exhibited a similar
296 trend as PPA in both the genotypes under control and HS (Fig. 2b). For downstream panicle level
297 gas exchange, we decided to use PPA as the normalizing parameter. The PPA and VC for TEJ-2

298 were lower than for TEJ-1 under both temperature conditions, confirming our direct observation
299 of TEJ-2 having a smaller panicle than TEJ-1 (Fig. 2a and 2b).

300

301 *Panicle photosynthetic response to heat stress is dynamic*

302 We next determined whether the gas exchange response of the primary panicle and its
303 corresponding flag leaf varied under the conditions described above (Fig. 3). A standard leaf
304 chamber of the open infra-red gas analyzer was used for the flag leaf. The foliar and non-foliar
305 photosynthetic measurements were conducted the same day as the panicle imaging. For TEJ-1 we
306 observed significantly lower ($p < 0.001$) stomatal conductance (g_{swleaf}) for the flag leaf under HS
307 compared to controls at both the time points (4 and 10 DAF) (Fig. S2). In contrast, flag leaf of
308 TEJ-2 exhibited higher g_{swleaf} at both 4 and 10 DAF under HS (Fig. S2). Since apparent
309 transpiration rate (E) is a function of stomatal conductance, E_{leaf} also remained significantly lower
310 ($p < 0.001$) for the TEJ-1 plants grown under HS at both time points compared to controls (Fig.
311 4a). TEJ-2 plants had higher E_{leaf} under HS (Fig. 4a). Consistent with stomatal conductance
312 (g_{swleaf}), recorded carbon assimilation (A_{leaf}) was significantly lower ($p < 0.001$) for TEJ-1 plants
313 under HS at both the time points (Fig. 4a). The carbon assimilation (A_{leaf}) rate of TEJ-2 did not
314 change significantly under HS at 4 and 10 DAF (Fig. 4a). Furthermore, we observed that leaf water
315 use efficiency (WUE_{leaf}) in TEJ-1 was significantly less under HS than control at both 4 and 10
316 DAF, with a decreasing trend (Fig. S7). In contrast, TEJ-2 exhibited an increasing trend for
317 WUE_{leaf} in HS and decreasing trend in control from 4 to 10 DAF (Fig. S7). This data suggest that
318 TEJ-1 exhibits greater gas exchange sensitivity in foliar tissue to HS relative to TEJ-2.

319 We next measured the panicle level photosynthetic response of TEJ-1 and TEJ-2 under HS using
320 a custom-built LI-6800-compatible cylindrical chamber for panicle measurements (Fig. 3). We
321 used PPA for normalizing panicle measurements across genotypes and treatments on a per unit
322 area basis (Fig. 1b). In TEJ-1, there was no difference between $A_{panicle}$ under control and HS at 4
323 DAF (Fig. 4b). However, the $A_{panicle}$ was reduced under HS at 10 DAF in TEJ-1. Like TEJ-1, no
324 difference in $A_{panicle}$ under control and HS was observed at 4 DAF in TEJ-2 (Fig. 4b). Notably, in
325 TEJ-2, the $A_{panicle}$ was higher under HS than control at 10 DAF (Fig. 4b-upper part). The panicle
326 level apparent transpiration rates ($E_{panicle}$) were higher under HS than control at 4 DAF in both
327 accessions (Fig. 4b). At 10 DAF, the apparent transpiration rate was similar under HS and control
328 in TEJ-1, and higher under HS than control in TEJ-2 (Fig. 4b-lower part). Additionally, panicle

329 water use efficiency ($WUE_{panicle}$) of TEJ-1 under HS remained significantly lower than control at
330 both the timepoints (Fig. S8). However, $WUE_{panicle}$ of TEJ-2 exhibited significant increase at 10
331 DAF under HS than control (Fig. S7). These photosynthetic measurements indicate that TEJ-1 and
332 TEJ-2 have contrasting responses under HS for A_{leaf} and $A_{panicle}$ at 10 DAF. Further, the percent
333 change observed in A_{leaf} and $A_{panicle}$ under HS when compared to corresponding controls at 10 DAF
334 (Fig. S3) quantified this genotypic difference. At 10 DAF, A_{leaf} and $A_{panicle}$ were reduced by 56%
335 and 26%, respectively, in TEJ-1 under HS compared to their corresponding controls. In contrast,
336 in TEJ-2, A_{leaf} and $A_{panicle}$ increased by 57% and 121% respectively, under HS relative to controls
337 (Fig. S3). Collectively, these analyses indicate the potential of our experimental approach
338 involving concurrent measurement of foliar and non-foliar photosynthetic parameters to discern
339 genotypic differences for photosynthetic parameters under heat stress.

340 Further, we investigated if the panicle-level photosynthetic parameters measured using the
341 cylinder-based chamber can be estimated from the digital traits extracted from the 3D
342 reconstructed panicles. For this we extracted the pixel color intensities from 3D-reconstructed
343 panicles to differentiate their response to HS. The 4 and 10 DAF measurements correspond to the
344 active grain filling phase when the panicle is predominantly green. Since green (G) pixel intensity
345 can be used as a proxy for panicle surface chlorophyll content, we estimated the proportion of
346 green pixels to the sum of red and green pixels [$G/(R+G)$] to determine changes in response to HS.
347 Under control conditions, TEJ-1 exhibited a decline in green pixel proportion from 4 to 10 DAF
348 (Fig. 2c). While under HS, no significant decline was observed from 4 to 10 DAF in green pixel
349 ratio in TEJ-1 (Fig. 2c). The proportion of green pixels decreased from 4 to 10 DAF in TEJ-2
350 under control conditions (Fig. 2c). These observations did not explain the change or lack of change
351 in photosynthetic parameters for both genotypes under control conditions. However, the proportion
352 of green pixels increased from 4 to 10 DAF in TEJ-2 under HS (Fig.2c). This observation was
353 consistent with the striking increase observed in $A_{panicle}$ in TEJ-2 at 10 DAF under HS (Fig. 4b-
354 upper part). As panicle approaches maturity, pixels are expected to shift towards R. Therefore, we
355 also analyzed the proportion of red pixels to the sum of red and green pixels [$R/(R+G)$]. In TEJ-1,
356 the proportion of red pixels increased from 4 to 10 DAF under control conditions, while it remained
357 similar between 4 and 10 DAF under HS (Fig. 2d). TEJ-2 also exhibited a similar trend as TEJ-1
358 for red pixels proportion under control conditions (Fig. 2d). However, the red pixel proportion was
359 higher in TEJ-2 than TEJ-1 under HS at both time points (Fig. 2d). Based on our analysis, whole

360 panicle level G pixel proportion does not correspond well with panicle gas exchange
361 measurements.

362

363 *Digital slicing of reconstructed panicles captures panicle level spatial variation*

364 The observed inconsistency between photosynthetic parameters and green pixel proportion,
365 promoted us to further examine the pixel color intensities by accounting for spatial variability
366 along the panicle length due to variable developmental stage of the seeds, resulting from
367 asynchronous fertilization. Therefore, we divided the 3D reconstructed panicle into ten equal
368 slices. Digital traits were obtained for individual slices (Fig. 1) and compared between control and
369 HS for each genotype (Fig. 5). We performed spatial analysis for VC and green pixel proportion
370 $[G/(R+G)]$ for both genotypes (Fig. 5 and S5). In TEJ-1, a gradient in green pixel proportion was
371 observed from top slices (slices 1-4) having higher green pixel proportion than lower slices (slices
372 5-10) at 4 DAF under control conditions (Fig. 5a). By the 10 DAF time point, the top slices (slices
373 1-4) had reduced green pixel proportion and the bottom slices (slices 5-10) had increased green
374 pixel proportion under control conditions in TEJ-1 (Fig. 5a). Unlike control conditions, a gradient
375 in green pixel proportion was observed with middle slices (slice 4-7) having higher proportion,
376 followed by bottom slices (slices 8-10), and then the top slices (slices 1-3) at 4 DAF under HS in
377 TEJ-1 (Fig. 5a). The green pixel proportion of upper slices (slices 1-4) increased at 10 DAF
378 compared with 4 DAF, whereas they were lower for most of the bottom slices (slices 5-10; except
379 slice 7) under HS in TEJ-1 (Fig. 5a). TEJ-2 also had a gradient in green pixel proportion under
380 control conditions at 4 DAF with the top slices (slices 1-4) having higher green pixel proportion
381 than the bottom slices (slices 5-10) (Fig. 5b). At 10 DAF, the top slices (slices 1-4) had a reduced
382 green pixel proportion, while the bottom slices (slices 5-10) had similar green pixel proportions as
383 those of 4 DAF under control conditions in TEJ-2 (Fig. 5b). A notable feature of the TEJ-2 under
384 HS was its ability to largely maintain a higher green pixel proportion for the bottom slices (slices
385 7-10) at 4 and 10 DAF relative to control values (Fig. 5b). At 10 DAF in TEJ-2, the green pixel
386 proportion for top slices (slices 1-6) increased slightly compared to 4 DAF under HS (Fig. 5b).
387 Collectively, variations in the green pixel proportion pattern obtained from slicing of 3D panicles
388 illustrates the spatial heterogeneity among the florets and its transition with progression of both
389 development and stress duration.

390

391 *Correlations between digital traits and photosynthetic measurements vary with genotypes*

392 We next examined the relationship among 3D reconstruction-derived features and photosynthetic
393 parameters for the genotypic responses to HS at 10 DAF. We selected the 10 DAF for this analysis
394 as we observed the most significant genotypic contrast at this time point under HS. We used the
395 digital traits (PPA, VC, and G) and photosynthetic measurements ($A_{panicle}$, $E_{panicle}$, A_{leaf} , E_{leaf}) to
396 perform pairwise correlation analysis separately for TEJ-1 and TEJ-2 under HS. The derived
397 digital traits, i.e., PPA, VC, and green pixel proportion, showed a strong positive correlation among
398 themselves and a negative correlation with A_{leaf} , $A_{panicle}$, and E_{leaf} in both genotypes (Fig. 6, green
399 boxes). Further, the correlation between some of the examined parameters exhibited contrasting
400 values in TEJ-1 and TEJ-2 (Fig. 6, blue boxes). Although these correlation values between
401 particular digital traits and photosynthetic parameters were not statistically significant, they still
402 suggest a divergent response for TEJ-1 and TEJ-2 under HS. For instance, in TEJ-1, the correlation
403 of $A_{panicle}$ with PPA, VC, and G was -0.42, -0.80, and -0.66, respectively (Fig. 6a, blue boxes),
404 while in TEJ-2, the correlation of $A_{panicle}$ with PPA, VC, and G were +0.43, +0.70, and +0.69,
405 respectively (Fig. 6b, blue boxes). These results suggest that despite having a larger panicle size
406 and higher pixel count under HS, TEJ-1 does not exhibit an increase in $A_{panicle}$, resulting in negative
407 correlation values. In TEJ-2, $A_{panicle}$ increases along with PPA, VC, and G under HS, resulting in
408 a positive correlation. Further, the correlation between $A_{panicle}$ and A_{leaf} in TEJ-1 and TEJ-2 was
409 +0.88 and -0.68, respectively (Fig. 6, blue box). These results suggest that in TEJ-1, both $A_{panicle}$
410 and A_{leaf} are decreasing under HS, leading to a positive correlation value (Fig. 2 and 6), while TEJ-
411 2 has higher $A_{panicle}$ and more stable A_{leaf} under HS, resulting in negative correlation (Fig. 2 and 6).

412

413 *Analysis of mature grain parameters of TEJ-1 and TEJ-2 under HS*

414 The digital traits from 3D reconstructed panicle and photosynthetic measurements indicate that
415 TEJ-1 and TEJ-2 have differential response to HS. We next asked if these observed differences at
416 early seed development stages translate to differences in grain traits at maturity. For this, we
417 imposed short (HS-I; 2-4 DAF) and long (HS-II; 2-10 DAF) duration HS and measured seed
418 length, width, weight, and fertility (Fig. S4a). Mature grain parameters of TEJ-1 and TEJ-2 did not
419 differ significantly different between control and HS-I, except for fertility (%), which was higher
420 in TEJ-2 after heat treatment (Fig. S4b). Under HS-II, fertility was significantly reduced in TEJ-1

421 but not in TEJ-2 (Fig. S4b). Seed length was not affected in TEJ-1 but increased under HS-II in
422 TEJ-2. A significant reduction in seed weight and width of marked seeds on the primary panicles
423 was observed for both TEJ-1 and 2 at HS-II compared to respective controls (Fig. S4b). The results
424 indicate that TEJ-1 and 2 exhibit differential tolerance to the longer duration heat stress (HS-II)
425 for marked seeds. At the whole plant level, the fertility and per plant grain weight were reduced
426 due to HS-I and HS-II in TEJ-1 compared to its control (Fig. 7a). However, these two parameters
427 were not affected for both heat treatments in TEJ-2. The whole plant level seed trait data suggests
428 that TEJ-2 exhibits greater heat tolerance even for seeds that were fertilized under heat stress
429 compared to TEJ-1. The marked seeds are distinct from whole plant level seeds as they are derived
430 from fertilization events that occur before the imposition of HS treatments.

431 **Discussion**

432 It is likely that the negative effects of HS on seed development results partially from disturbance
433 in photosynthesis not only in foliar tissues, but also in non-foliar tissues, as well from the dynamic
434 interactions between these two photosynthate sources. To explore these questions, we developed
435 and tested a novel and more precise method to non-destructively measure rice panicle
436 photosynthetic parameters. Our hypothesis was that this approach, combined with concurrent foliar
437 measurements by traditional methods, would enhance our understanding of the photosynthetic
438 response to HS. Further, we postulated that this method could uncover differences between rice
439 lines that differ in their HS response during reproductive development. Such comparative analyses
440 could eventually help explain why grain fill in some rice accessions is less affected by HS than
441 others. We determined the relative rates of gas exchange between flag leaf and panicle under HS
442 during grain filling stage, the effect of altered carbon fixation (of flag leaf and panicle) due to HS
443 on the final grain yield parameters and distinguish the differential physiological response of two
444 genotypes under HS. In addition to photosynthetic measurements, we also assessed panicle level
445 digital traits to track developmental dynamics along the panicle length under control and HS
446 conditions. For this, we digitally partitioned the 3D reconstructed panicle into ten equal slices and
447 extracted digital traits for each slice. The spatial perspective of the 3D reconstructed panicle
448 enabled us to discern differences between TEJ-1 and TEJ-2 heat stress response at greater
449 resolution (Fig. 5). The analysis of voxel count (VC) and projected panicle area (PPA) from the
450 whole panicles indicated an increasing trend from 4 to 10 DAF in both genotypes under optimal
451 conditions (Fig. 2a & 2b). The spatiotemporal characterization of the panicle slices was able to

452 differentiate responses of the two genotypes that were not evident from whole panicle traits. For
453 instance, whole 3D panicle of TEJ-1 under HS did not exhibit a significant change in the green
454 pixel proportion from 4 to 10 DAF (Fig. 2c). However, sliced 3D panicle results indicate that green
455 pixel proportion of lower (proximal) slices was higher at 4 DAF whereas upper (distal) slices were
456 higher at 10 DAF (Fig. 5a). For TEJ-2, we observed more stable green pixel spatial profile when
457 comparing the 4 and 10 DAF under HS. TEJ-2 slicing results show that the proximal panicle slices
458 (slices 7-10) do not exhibit a drop in the green pixel intensity at 10 DAF under HS (Fig. 5b). This
459 is in contrast with the proximal slices (8-10) in the TEJ-1 at 10 DAF. It is plausible that observed
460 increase in $A_{panicle}$ at 10 DAF under HS in TEJ-2 could be primarily due to proximal spikelets that
461 “stay green” for longer duration. Alternatively, the panicle architecture of TEJ-2 may be different
462 from TEJ-1 in maintaining growth in proximal part, reflected in largely stable values across time
463 and treatments.

464 The digital traits derived from 3D reconstructed panicles were able to detect variations in
465 developmental progression of the two genotypes under HS. Since developing grain acts as the
466 active sink tissue, the progression in grain development depends upon accumulation and utilization
467 of the photoassimilates. To examine the source-sink relationship and its effect on grain
468 development, we measured photosynthetic parameters for the flag leaf and primary panicle
469 simultaneously. Apart from the major photosynthetic parameters impacting carbon fixation,
470 parameters like vapor pressure deficit (VPD) are known to increase under HS, and hence are a
471 factor for consideration (De Boeck *et al.*, 2010; Grossiord *et al.*, 2020). Our results show a higher
472 leaf VPD for the plants exposed to HS, indicating a greater leaf-atmosphere diffusion gradient
473 (Fig.S2). At higher VPD , plants tend to lose more water and trigger stomatal closure to maintain
474 plant water status under limited water conditions (De Boeck *et al.*, 2010; Grossiord *et al.*, 2020;
475 Moore *et al.*, 2021). However, if water availability and VPD are not restrictive factors, high
476 temperature can induce guard cell expansion which facilitates stomatal opening to trigger
477 evaporative cooling of the leaf (Faralli *et al.* 2019; Tricker *et al.* 2018; Kostaki *et al.*, 2020). The
478 two genotypes in this study showed a contrasting response in foliar gas exchange parameters on
479 exposure to HS under similar growth conditions, including water availability and VPD (Fig. 4 and
480 S2). For instance, reduction in leaf stomatal conductance, apparent transpiration rate, and carbon
481 assimilation was observed in TEJ-1 under HS even though plants were growing in well-watered
482 conditions. In contrast, TEJ-2 maintains higher apparent transpiration rate, stomatal conductance,

483 and carbon assimilation under longer duration HS, suggesting that there may be a temperature
484 dependent or independent stomatal response difference between the two genotypes. This could be
485 due to genotypic variation in biomechanical elasticity of the guard cell complex. Alternatively,
486 TEJ-1 may lack the hydraulic structure to sustain water movement under high *VPD* conditions,
487 resulting in differential ABA accumulation in the guard cells.

488 The non-foliar, panicle-based photosynthetic measurements indicated that net CO₂ assimilation
489 (*A_{panicle}*) for both genotypes was similar between optimal and HS conditions at 4 DAF (Fig. 4b).
490 However, *A_{panicle}* exhibited a contrasting response in TEJ-1 and TEJ-2 under HS at 10 DAF. TEJ-
491 1 showed a decline and TEJ-2 showed an increase in *A_{panicle}* under HS compared to their respective
492 controls at 10 DAF (Fig. 4b). Notably, the apparent transpiration rate for the TEJ-2 declined under
493 HS but the *A_{panicle}* increased for 10 DAF panicles. Therefore, estimated WUE for TEJ-2 was also
494 significantly higher than the optimal conditions at 10 DAF (Fig. S8). This decoupling of *A_{panicle}*
495 from the apparent transpiration rate in TEJ-2 under HS is intriguing as it likely promotes carbon
496 assimilation rather than evaporative cooling of the panicle.

497 The photosynthetic parameters measured for two genotypes were consistent with plant-level grain
498 parameters. For instance, TEJ-1, which exhibited a decline in assimilation rate (*A_{panicle}* and *A_{leaf}*)
499 measured during the grain filling stage, also had significantly reduced mature grain weight and
500 fertility parameters (Fig. 4 and 7). TEJ-2 had an enhanced assimilation rate (*A_{panicle}* and *A_{leaf}*) under
501 HS at 10 DAF and showed no significant change in mature grain weight and fertility parameters
502 at whole-plant level (Fig. 4 and 7). In TEJ-1, there was a greater percent decrease in *A_{leaf}* (-57%)
503 than in *A_{panicle}* (-26%) at 10 DAF under HS as compared to respective controls. In contrast, in TEJ-
504 2 the percent increase in *A_{leaf}* (57%) was considerably less than in *A_{panicle}* (121%) in response to
505 HS relative to control values. The higher *A_{panicle}* for TEJ-2 under HS at 10 DAF is also consistent
506 with the more stable spatial profile of TEJ-2 for green pixel proportion under HS relative to TEJ-
507 1, especially in the proximal end of panicles.

508 *Conclusion*

509 This work shows the potential value of combining foliar and non-foliar physiological
510 measurements to examine dynamic heat stress response in rice, and to identify genotypic
511 differences in this response. By measuring temporal dynamics along the panicle length, we were
512 also able to discern spatial differences under heat stress. This improved non-destructive approach

513 combines 3D imaging, photosynthetic measurements, and grain physiology, and could be used to
514 gain a spatiotemporal perspective on multiple stress responses and in a variety of cereal species
515 bearing compact inflorescences.

516 **Acknowledgements**

517 We would like to thank Prof. Timothy Arkebauer at University of Nebraska-Lincoln and Dr. Harel
518 Bacher at Cornell University for their suggestions to improve the manuscript. We would also like
519 to thank Jeremy Hiller for helping in trouble-shooting the technical issues while performing
520 experiments with the LiCor instrument.

521 **Author contributions**

522 HW, BKD, and JSD wrote the manuscript with contributions from all authors. JSD, BKD, and PP
523 performed the experiments and analyzed the results. JH designed and built the customized
524 cylinder. JSD and BKD calibrated and tested the customized cylinder. TG and HY performed the
525 image analysis. TA and PAS critically reviewed and analyzed the work. All authors read and
526 approved the manuscript.

527 **References**

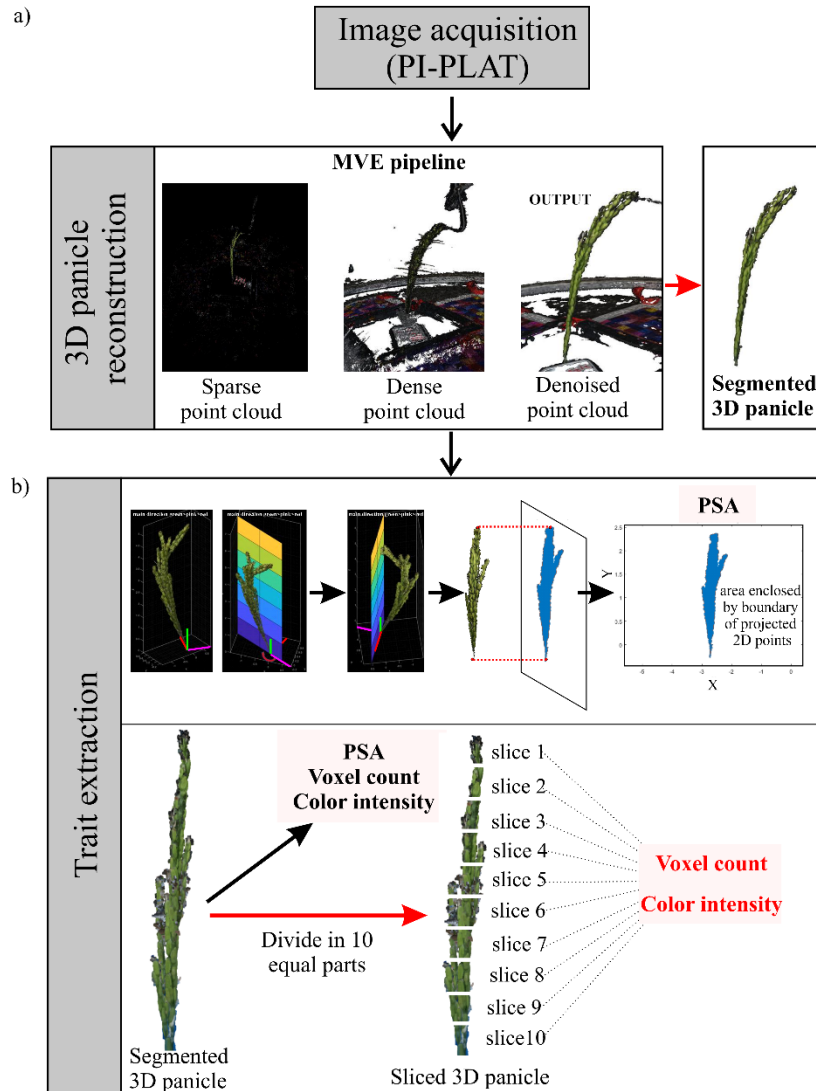
- 528 **Abdelrahman M, Burritt DJ, Gupta A, Tsujimoto H, Tran L-SP. 2020.** Heat stress effects on
529 source–sink relationships and metabolome dynamics in wheat (C Foyer, Ed.). *Journal of*
530 *Experimental Botany* **71**: 543–554.
- 531 **Ali F, Waters DLE, Ovenden B, Bundock P, Raymond CA, Rose TJ. 2019.** Australian rice
532 varieties vary in grain yield response to heat stress during reproductive and grain filling stages.
533 *Journal of Agronomy and Crop Science* **205**: 179–187.
- 534 **Arshad MS, Farooq M, Asch F, Krishna JSV, Prasad PVV, Siddique KHM. 2017.** Thermal
535 stress impacts reproductive development and grain yield in rice. *Plant physiology and*
536 *biochemistry : PPB* **115**: 57–72.
- 537 **Austin RB, Edrich JA, Ford MA, Blackwell RD. 1977.** *The Fate of the Dry Matter,*
538 *Carbohydrates and 14 C Lost from the Leaves and Stems of Wheat during Grain Filling.*
- 539 **Bidinger F, Musgrave R, Nature RF-, 1977 undefined.** *Contribution of stored pre-anthesis*
540 *assimilate to grain yield in wheat and barley.*
- 541 **De Boeck HJ, Dreesen FE, Janssens IA, Nijs I. 2010.** Climatic characteristics of heat waves
542 and their simulation in plant experiments. *Global Change Biology* **16**: 1992–2000.
- 543 **Chang TG, Song QF, Zhao HL, Chang S, Xin C, Qu M, Zhu XG. 2020.** An in situ approach
544 to characterizing photosynthetic gas exchange of rice panicle. *Plant Methods* **16**: 92.

- 545 **Chen C, Begcy K, Liu K, Folsom JJ, Wang Z, Zhang C, Walia H. 2016.** Heat stress yields a
546 unique MADS box transcription factor in determining seed size and thermal sensitivity. *Plant*
547 *Physiology* **171**: 606–622.
- 548 **Cohen-Or D, Kaufman A. 1995.** Fundamentals of surface voxelization. *Graphical models and*
549 *image processing* **57**: 453–461.
- 550 **Dhatt, B. K., Abshire, N., Paul, P., Hasanthika, K., Sandhu, J., Zhang, Q., Obata, T.,**
551 **&Walia, H. 2019.** Metabolic Dynamics of Developing Rice Seeds Under High Night-Time
552 Temperature Stress. *Frontiers in Plant Science*, 10(November), 1–16.
- 553 **Dhatt BK, Paul P, Sandhu J, Hussain W, Irvin L, Zhu F, Adviento-Borbe MA, Lorence A,**
554 **Staswick P, Yu H, et al. 2021.** Allelic variation in rice Fertilization Independent Endosperm 1
555 contributes to grain width under high night temperature stress. *New Phytologist* **229**: 335–350.
- 556 **Djanaguiraman M, Science PP-C, 2013 undefined. 2013.** High Day- or Nighttime
557 Temperature Alters Leaf Assimilation, Reproductive Success, and Phosphatidic Acid of Pollen
558 Grain in Soybean. *Wiley Online Library* **53**: 1594–1604.
- 559 **Faralli M, Matthews J, biology TL-C opinion in plant, 2019 undefined.** Exploiting natural
560 variation and genetic manipulation of stomatal conductance for crop improvement. *Elsevier*.
- 561 **Ferguson JN, Tidy AC, Murchie EH, Wilson ZA, John Ferguson CN. 2021.** The potential of
562 resilient carbon dynamics for stabilizing crop reproductive development and productivity during
563 heat stress. *Wiley Online Library* **44**: 2066–2089.
- 564 **Folsom JJ, Begcy K, Hao X, Wang D, Walia H. 2014.** Rice fertilization-independent
565 Endosperm1 regulates seed size under heat stress by controlling early endosperm development.
566 *Plant Physiology* **165**: 238–248.
- 567 **Fuhrmann S, Goesele M. 2014.** Floating scale surface reconstruction. *ACM Transactions on*
568 *Graphics* **33**: 1–11.
- 569 **Fuhrmann S, Langguth F, Goesele M. 2014.** MVE – A Multi-View Reconstruction
570 Environment. *EUROGRAPHICS Workshops on Graphics and Cultural Heritage*.
- 571 **Gao B, Hu S, Jing L, Niu X, Wang Y, Zhu J, Wang Y, Yang L. 2021a.** Alterations in Source-
572 Sink Relations Affect Rice Yield Response to Elevated CO₂: A Free-Air CO₂ Enrichment
573 Study. *Frontiers in Plant Science* **12**.
- 574 **Gao T, Zhu F, Paul P, Sandhu J, Akrofi Doku H, Sun J, Pan Y, Staswick P, Walia H, Yu H,**
575 **et al. 2021b.** remote sensing Novel 3D Imaging Systems for High-Throughput Phenotyping of
576 Plants.
- 577 **Gitelson AA, Kaufman YJ, Stark R, Rundquist D. 2002.** Novel algorithms for remote
578 estimation of vegetation fraction. *Remote Sensing of Environment* **80**: 76–87.
- 579 **Grossiord C, Buckley TN, Cernusak LA, Novick KA, Poulter B, Siegwolf RTW, Sperry JS,**
580 **McDowell NG. 2020.** Plant responses to rising vapor pressure deficit. *New Phytologist* **226**:
581 1550–1566.
- 582 **Grundbacher FJ. 1963.** The physiological function of the cereal awn. *Springer*.

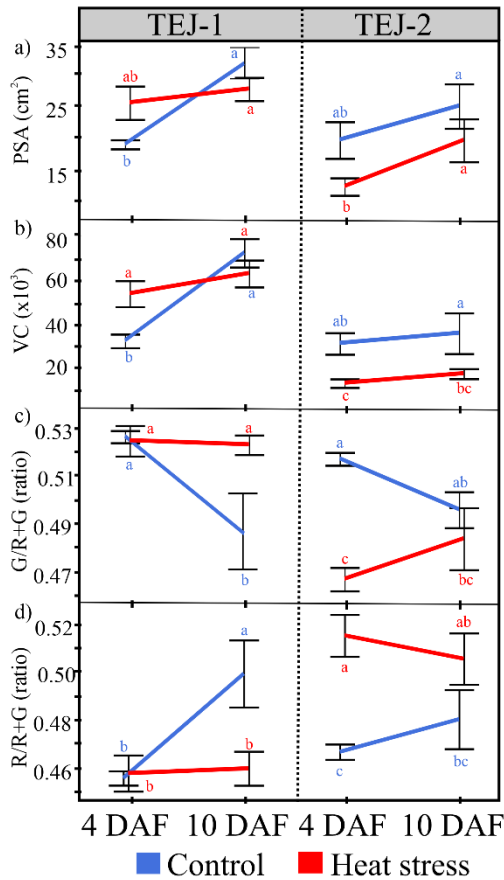
- 583 **Imaizumi N, Usuda H, Nakamoto H, Ishihara K. 1990.** *Changes in the Rate of Photosynthesis*
584 *during Grain Filling and the Enzymatic Activities Associated with the Photosynthetic Carbon*
585 *Metabolism in Rice Panicles.*
- 586 **Inoue T, Inanaga S, Sugimoto Y, An P, Eneji AE. 2004.** *Effect of drought on ear and flag leaf*
587 *photosynthesis of two wheat cultivars differing in drought resistance.*
- 588 **Jagadish SVK. 2020.** Heat stress during flowering in cereals – effects and adaptation strategies.
589 *New Phytologist* **226**: 1567–1572.
- 590 **Jagadish SVK, Craufurd PQ, Wheeler TR. 2007.** High temperature stress and spikelet fertility
591 in rice (*Oryza sativa* L.). *Journal of Experimental Botany* **58**: 1627–1635.
- 592 **Kadan RS, Bryant RJ, Miller JA. 2008.** Effects of Milling on Functional Properties of Rice
593 Flour. *Journal of Food Science* **73**: E151–E154.
- 594 **Khush GS. 2005.** What it will take to Feed 5.0 Billion Rice consumers in 2030. *Plant Molecular*
595 *Biology* **59**: 1–6.
- 596 **Khush GS, Jena KK. 2009.** Current Status and Future Prospects for Research on Blast
597 Resistance in Rice (*Oryza sativa* L.). In: *Advances in Genetics, Genomics and Control of Rice*
598 *Blast Disease*. Dordrecht: Springer Netherlands, 1–10.
- 599 **Kong LA, Xie Y, Sun MZ, Si JS, Hu L. 2016.** Comparison of the photosynthetic characteristics
600 in the pericarp and flag leaves during wheat (*Triticum aestivum* L.) caryopsis development.
601 <http://ps.ueb.cas.cz/doi/10.1007/s11099-015-0153-y.html> **54**: 40–46.
- 602 **Kostaki KI, Coupel-Ledru A, Bonnell VC, Gustavsson M, Sun P, McLaughlin FJ, Fraser**
603 **DP, McLachlan DH, Hetherington AM, Dodd AN, et al. 2020.** Guard Cells Integrate Light
604 and Temperature Signals to Control Stomatal Aperture. *Plant Physiology* **182**: 1404–1419.
- 605 **Li Z, Pinson SRM, Stansel JW, Paterson AH. 1998.** Genetic dissection of the source-sink
606 relationship affecting fecundity and yield in rice (*Oryza sativa* L.). *Molecular Breeding* **4**: 419–
607 426.
- 608 **Lisle AJ, Martin M, Fitzgerald MA. 2000.** Chalky and Translucent Rice Grains Differ in
609 Starch Composition and Structure and Cooking Properties. *Cereal Chemistry Journal* **77**: 627–
610 632.
- 611 **Lubis I, Shiraiwa T, Ohnishi M, Horie T, Inoue N. 2003.** Contribution of sink and source
612 sizes to yield variation among rice cultivars. *Plant Production Science* **6**: 119–125.
- 613 **Maydup ML, Antonietta M, Guiamet JJ, Tambussi EA. 2012.** The contribution of green parts
614 of the ear to grain filling in old and modern cultivars of bread wheat (*Triticum aestivum* L.):
615 Evidence for genetic gains over the past century. *Field Crops Research* **134**: 208–215.
- 616 **Moore CE, Meacham-Hensold K, Lemonnier P, Slattery RA, Benjamin C, Bernacchi CJ,**
617 **Lawson T, Cavanagh AP. 2021.** The effect of increasing temperature on crop photosynthesis:
618 from enzymes to ecosystems (R Hancock, Ed.). *Journal of Experimental Botany* **72**: 2822–2844.
- 619 **Muthayya S, Sugimoto JD, Montgomery S, Maberly GF. 2014.** An overview of global rice
620 production, supply, trade, and consumption. *Annals of the New York Academy of Sciences* **1324**:

- 621 7–14.
- 622 **Paul, P., Dhatt, B. K., Miller, M., Folsom, J. J., Wang, Z., Krassovskaya, I., Liu, K.,**
623 **Sandhu, J., Yu, H., Zhang, C., Obata, T., Staswick, P., & Walia, H. (2020).** *MADS78 and*
624 *MADS79 Are Essential Regulators of Early Seed Development in Rice.* *Plant Physiology,*
625 *182(2), 933–948.*
- 626 **Paul P, Dhatt BK, Sandhu J, Hussain W, Irvin L, Morota G, Staswick P, Walia H. 2020.**
627 **Divergent phenotypic response of rice accessions to transient heat stress during early seed**
628 **development.** *Plant Direct* **4:** 1–13.
- 629 **Peng S, Huang J, ... JS-P of the, 2004 undefined.** Rice yields decline with higher night
630 temperature from global warming. *National Acad Sciences.*
- 631 **Pokharel M, Chiluwal A, Stamm M, Min D, Rhodes D, Jagadish SVK. 2020.** High night-
632 time temperature during flowering and pod filling affects flower opening, yield and seed fatty
633 acid composition in canola. *Journal of Agronomy and Crop Science* **206:** 579–596.
- 634 **Prasad P, Bheemanahalli R, Research SJ-FC, 2017 undefined.** Field crops and the fear of
635 heat stress—opportunities, challenges and future directions. *Elsevier.*
- 636 **Prasad PV V., Pisipati SR, Ristic Z, Bukovnik U, Fritz AK. 2008.** Impact of Nighttime
637 Temperature on Physiology and Growth of Spring Wheat. *Crop Science* **48:** 2372–2380.
- 638 **Sanchez-Bragado R, Molero G, Reynolds MP, Araus JL. 2016.** Photosynthetic contribution
639 of the ear to grain filling in wheat: a comparison of different methodologies for evaluation.
640 *Journal of Experimental Botany* **67:** 2787–2798.
- 641 **Sandhu J, Zhu F, Paul P, Gao T, Dhatt BK, Ge Y, Staswick P, Yu H, Walia H.** PI-Plat: a
642 high-resolution image-based 3D reconstruction method to estimate growth dynamics of rice
643 inflorescence traits.
- 644 **Schrader SM, Wise RR, Wacholtz WF, Ort DR, Sharkey TD. 2004.** Thylakoid membrane
645 responses to moderately high leaf temperature in Pima cotton. *Plant, Cell and Environment* **27:**
646 *725–735.*
- 647 **Simkin AJ, Faralli M, Ramamoorthy S, Lawson T. 2020.** Photosynthesis in non-foliar tissues:
648 implications for yield. *The Plant Journal* **101:** 1001–1015.
- 649 **Sreenivasulu N, Butardo VM, Misra G, Cuevas RP, Anacleto R, Kishor PBK. 2015.**
650 **Designing climate-resilient rice with ideal grain quality suited for high-temperature stress.**
651 *Journal of Experimental Botany* **66:** 1737–1748.
- 652 **Tambussi EA, Bort J, Guamet JJ, Nogués S, Araus JL. 2007.** The Photosynthetic Role of
653 Ears in C3 Cereals: Metabolism, Water Use Efficiency and Contribution to Grain Yield.
654 <https://doi.org/10.1080/07352680601147901> **26:** 1–16.
- 655 **Tambussi EA, Maydup ML, Carrión CA, Guamet JJ, Araus JL. 2021.** Ear photosynthesis
656 in C3 cereals and its contribution to grain yield: methodologies, controversies, and perspectives.
657 *Journal of Experimental Botany* **72:** 3956–3970.
- 658 **Tricker P, ElHabt A, ... JS-J of experimental, 2018 undefined.** The physiological and

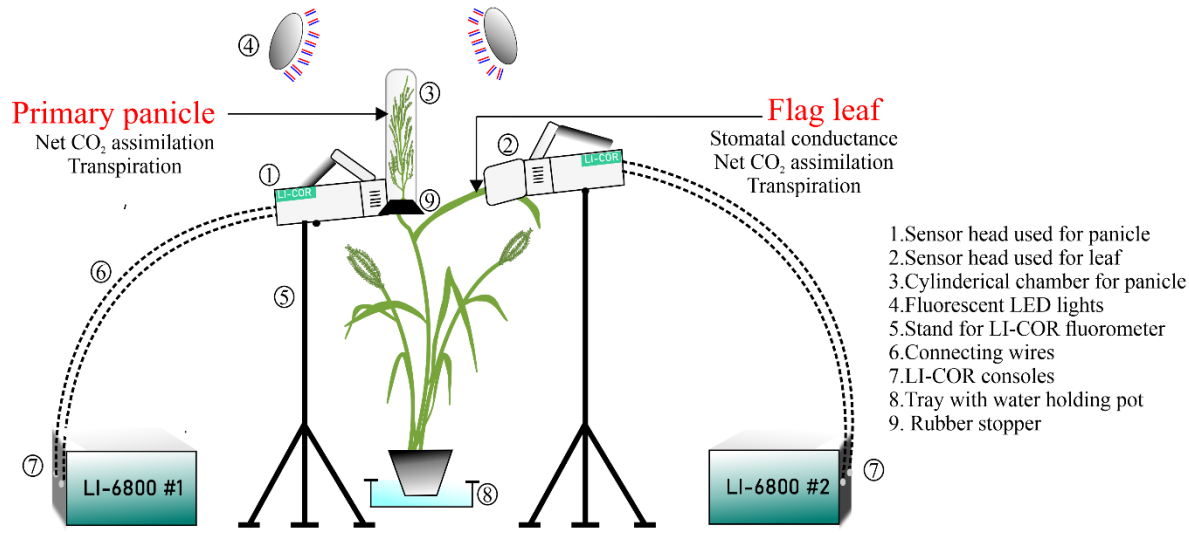
- 659 genetic basis of combined drought and heat tolerance in wheat. *academic.oup.com*.
- 660 **Walker BJ, Vanlooche A, Bernacchi CJ, Ort DR. 2016.** The Costs of Photorespiration to Food
661 Production Now and in the Future. *Annual Review of Plant Biology* **67**: 107–129.
- 662 **Wang Y, Pang Y, Chen K, Zhai L, Shen C, Wang S, Xu J. 2020.** Genetic bases of source-,
663 sink-, and yield-related traits revealed by genome-wide association study in Xian rice. *Crop*
664 *Journal* **8**: 119–131.
- 665 **Zhang CX, Feng BH, Chen TT, Fu WM, Li HB, Li GY, Jin QY, Tao LX, Fu GF. 2018.** Heat
666 stress-reduced kernel weight in rice at anthesis is associated with impaired source-sink
667 relationship and sugars allocation. *Environmental and Experimental Botany* **155**: 718–733.
- 668 **Zhao C, Liu B, Piao S, Wang X, Lobell DB, Huang Y, Huang M, Yao Y, Bassu S, Ciaais P, et**
669 **al. 2017.** Temperature increase reduces global yields of major crops in four independent
670 estimates. *Proceedings of the National Academy of Sciences of the United States of America* **114**:
671 9326–9331.
- 672 **Zhu F, Paul P, Hussain W, Wallman K, Dhatt BK, Sandhu J, Irvin L, Morota G, Yu H,**
673 **Walia H, et al. 2021a.** SeedExtractor : An Open-Source GUI for Seed Image Analysis. *Frontiers*
674 *in Plant Science* **11**: 1–10.
- 675 **Zhu F, Saluja M, Dharni JS, Paul P, Sattler SE, Staswick P, Walia H, Yu H. 2021b.**
676 PhenImage : An open-source graphical user interface for plant image analysis . *The Plant*
677 *Phenome Journal* **4**.
- 678
- 679 **Figure legends**



681 **Figure 1.** (a) Workflow for reconstruction of 3D panicle from Multiview images using PI-Plat
682 imaging platform. (b) Trait extraction from the reconstructed 3D panicle. The upper panel shows
683 the extracted projected panicle area (PPA) from boundary of projected 2D points. The lower
684 panel shows the traits derived from the segmented 3D panicle and sliced 3D panicle (voxel count
685 and color intensity). Slice 1 corresponds to the top-most slice and slice 10 corresponds to the
686 bottom-most slice of the 3D panicle.

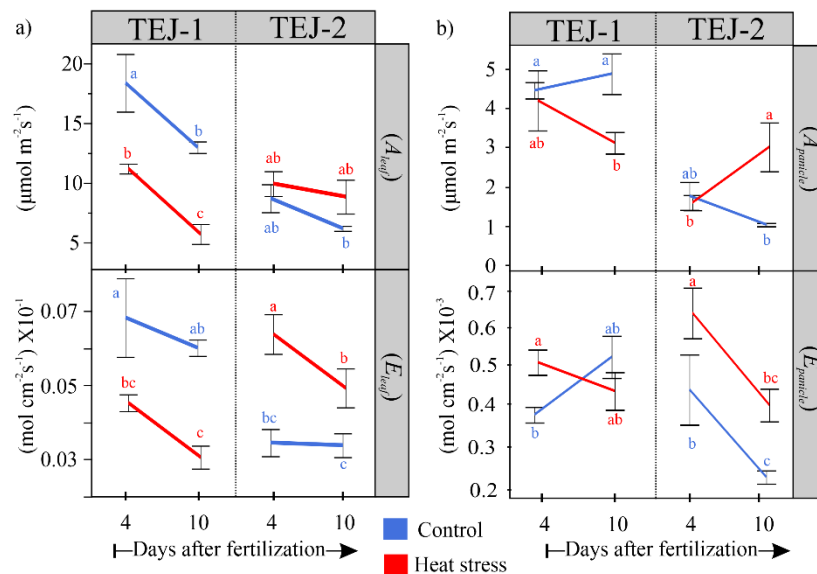


688 **Figure 2.** Digital trait analysis from 3D reconstructed panicles of TEJ-1 and TEJ-1 under control
 689 (28/23°C; day/night) and HS (36/32°C; day/night). HS was imposed 1 DAF and the traits were
 690 measured at 4 DAF and 10 DAF. (a) PPA (Projected panicle area) in cm², (b) VC (Voxel count)
 691 representing the point count in a 3D plane, (c) Ratio of green pixels (G) to the sum of red and
 692 green pixels (R+G) in a 3D plane, (d) Ratio of red pixels (R) to the sum of red and green pixels
 693 (R+G) in a 3D plane. n = 3-4 plants per data point. For statistical analysis, student's t-test was
 694 used to compare respective control and heat stress ($\alpha = 0.05$). Significant differences are
 695 indicated by different letters. Error bars represent \pm SE.

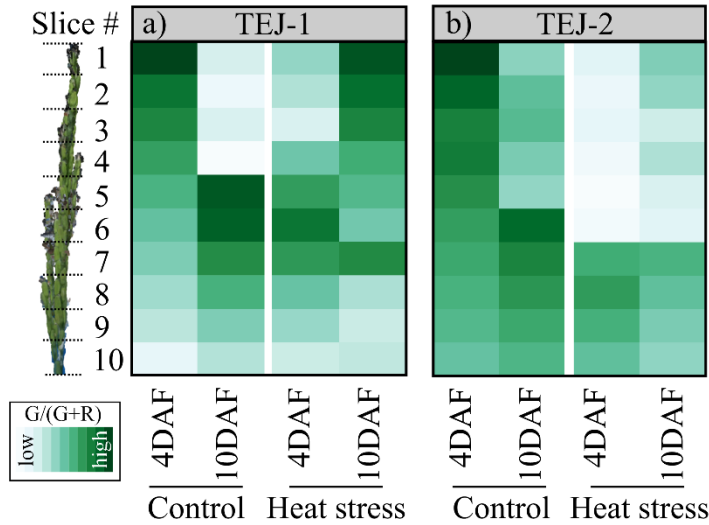


697 **Figure 3.** Pictorial representation of the setup used for measuring gas exchange parameters of
 698 flag leaf and primary panicle simultaneously using two LI-6800s. The photosynthetic parameters
 699 obtained from leaf and panicle that are used for comparative analysis in the study are mentioned
 700 in the picture. Numbers represent details of each part of the setup.

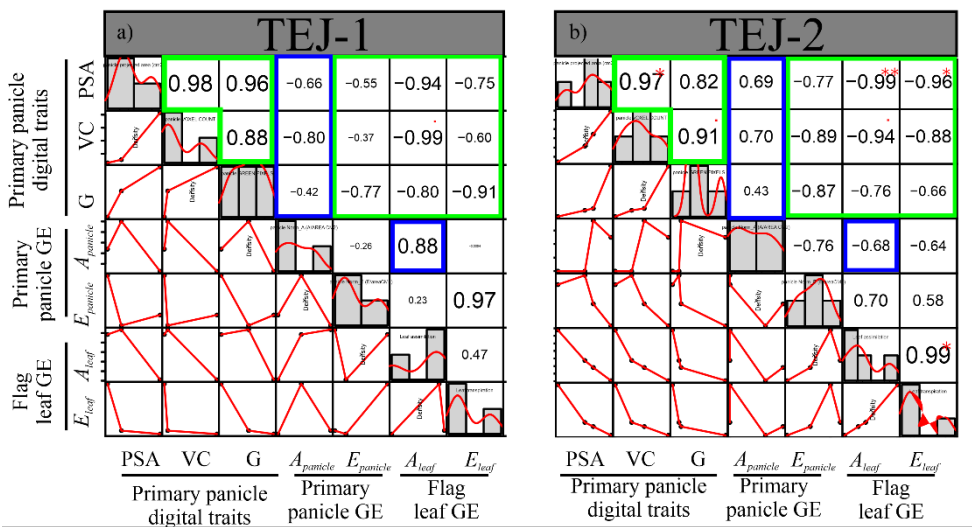
701



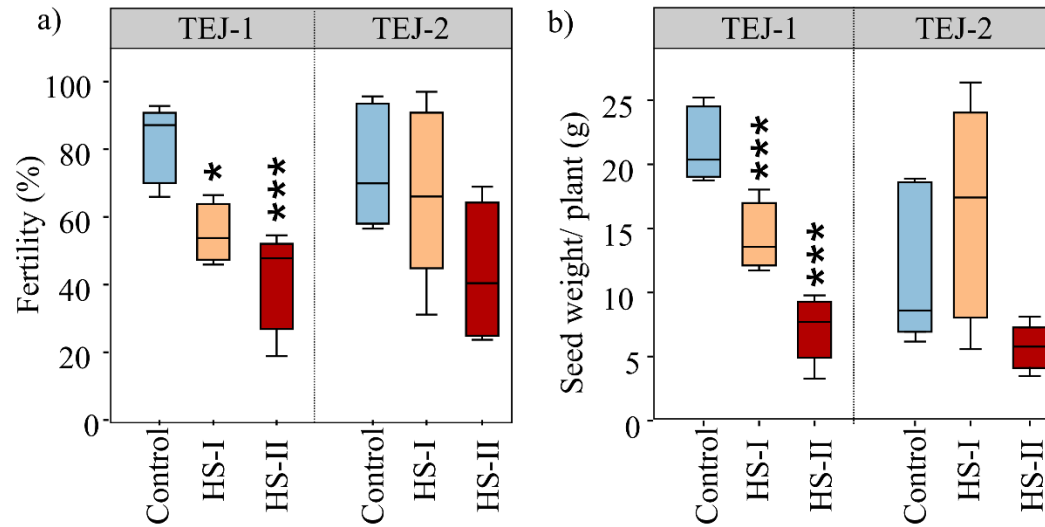
703 **Figure 4.** Gas exchange parameters for TEJ-1 and TEJ-2 (a) Flag leaf and (b) Panicle developing
 704 under control and heat stress conditions at 4 and 10 DAF (A: Net CO₂ assimilation; E:
 705 Transpiration). N=3-4 plants per data point. For statistical analysis, student's t-test was used to
 706 compare respective control and heat stress values of each of the traits ($\alpha = 0.05$). Significant
 707 differences are indicated by different letters. Error bars represent \pm SE. Blue and red color
 708 represents control and heat stress, respectively.



710 **Figure 5.** Shifts in green pixel intensity resolved into 3D slices using the panicle point cloud (a)
 711 TEJ-1 and (b) TEJ-2. Progression of color from white to green in the heat map represents increase
 712 in green pixel intensity, which is a proxy for chlorophyll content of panicle surface. N=3-4 plants
 713 per data point. Respective values from each slice of all the replicates were averaged to make the
 714 final heat map. Control and heat stress values of green pixel intensity for the genotypes are on
 715 same scale to show the temporal and spatial changes.



717 **Figure 6.** Correlation of primary panicle digital traits, primary panicle gas exchange (GE)
 718 parameters and flag leaf GE parameters at 10 DAF under HS in (a) TEJ-1 and (b) TEJ-2.
 719 Histograms and red lines represent each trait's distribution. Green colored boxes indicate similar
 720 type of correlation in TEJ-1 and TEJ-2 for the respective traits. Blue colored boxes represent
 721 contrasting correlation values in TEJ-1 and TEJ-2 for underlying traits. PSA: projected surface
 722 area, VC: voxel count, G: proportion of green pixel intensity, $A_{panicle}$: Net CO₂ assimilation of
 723 primary panicle, $E_{panicle}$: Transpiration of primary panicle, A_{leaf} : Net CO₂ assimilation of flag leaf,
 724 E_{leaf} : Transpiration of flag leaf, GE: gas exchange. (**, $p < 0.01$; * $p < 0.05$.)

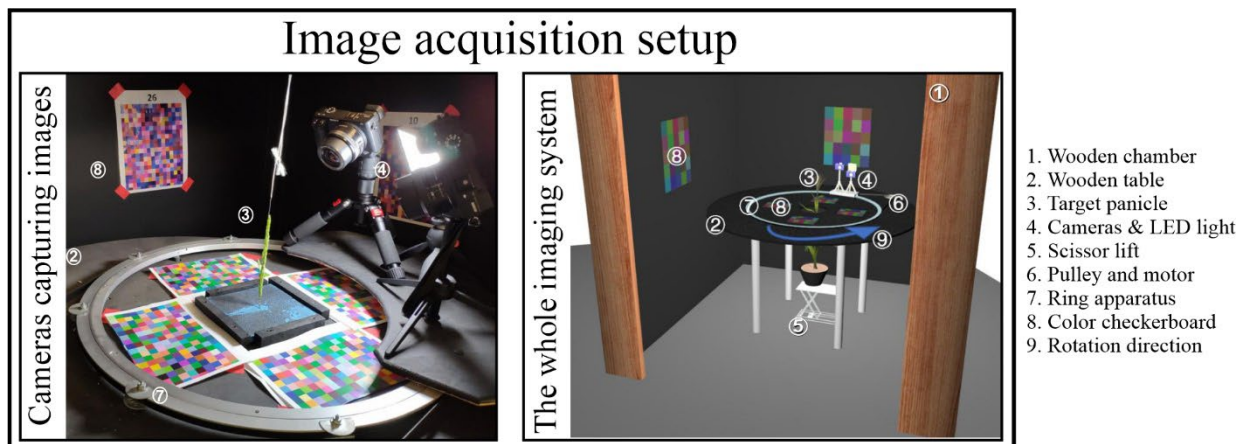


726 **Figure 7.** Impact of heat stress on mature seeds at whole plant level in TEJ-1 and TEJ-2 developing
 727 under control and heat stress (HS) conditions during grain filling. HS-I and HS-II refer to the
 728 duration of imposed HS i.e., 1-4 DAF (HS-I) and 1-10 DAF (HS-II). a) Quantification of spikelet
 729 fertility (%) and b) seed weight in grams at the whole plant level evaluated at time of physiological
 730 maturity. Box plots show the median and the upper quartiles and black dots signify outliers
 731 (5th/95th percentile). N= 1500-3500 seeds from 4-6 plants per data point. For statistics, t-test was
 732 used to compare heat stressed mature seeds with respective controls (***, p < 0.001; **, p < 0.01;
 733 * p < 0.05.)

734

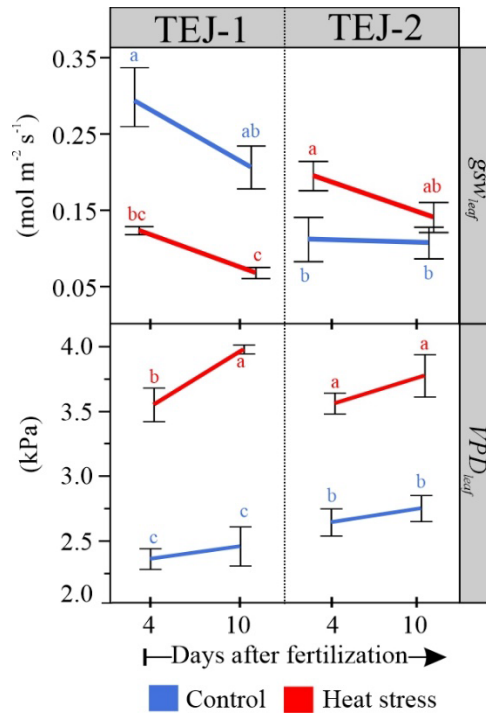
735 Supporting information

736



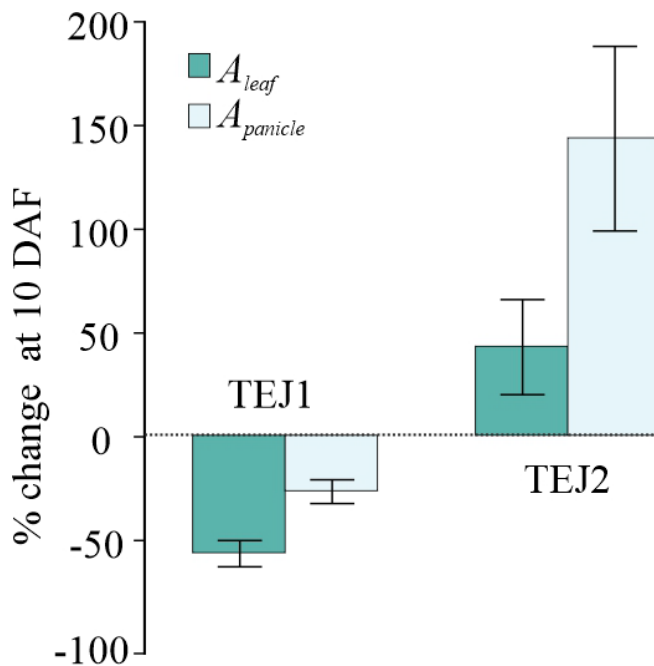
738 **Figure S1.** Image acquisition setup using PI-Plat imaging platform.

739

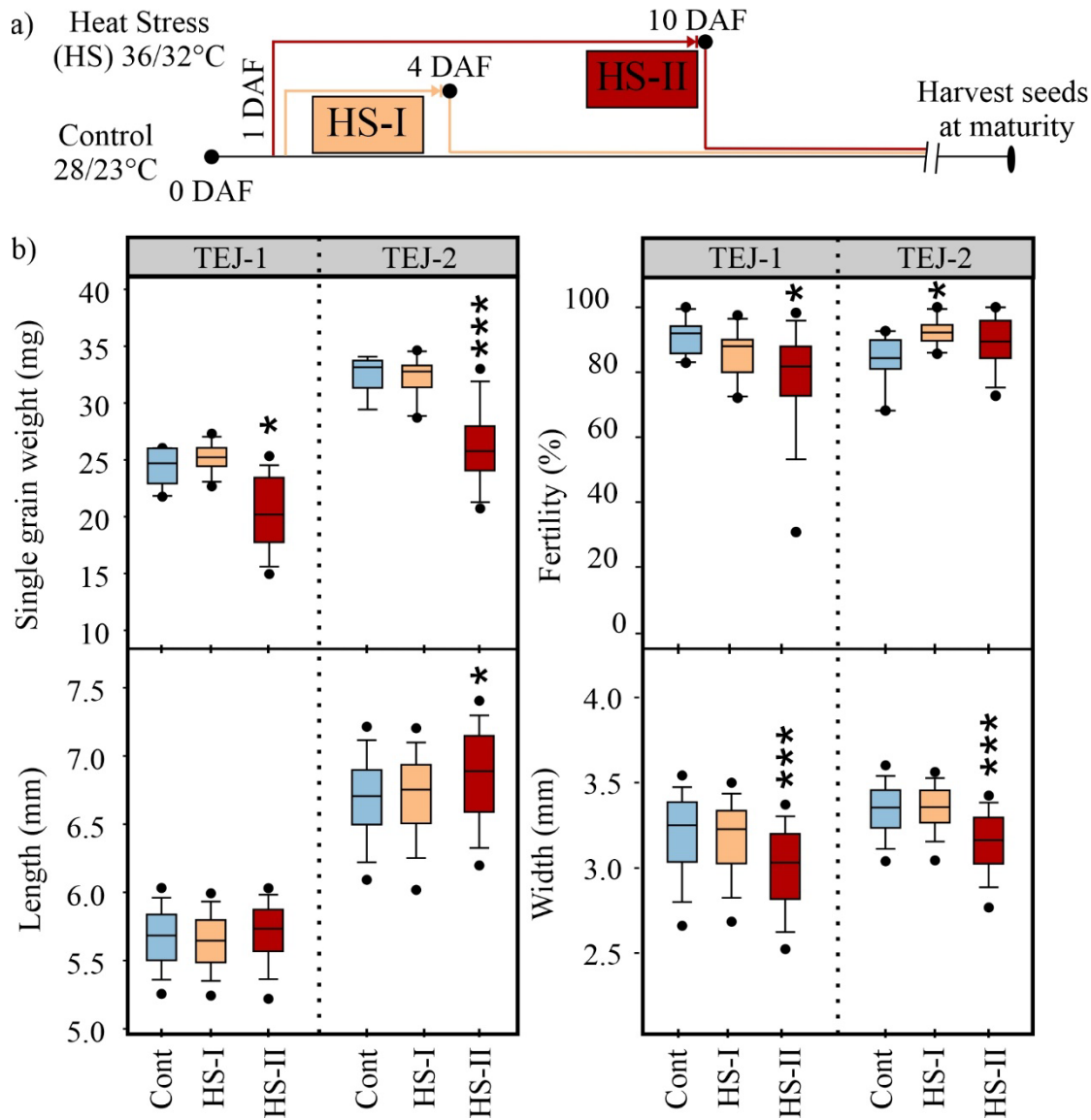


741 **Figure S2.** Stomatal conductance (g_{sw}) and vapor pressure deficit (VPD) of flag leaf of TEJ-1 and
 742 TEJ-2 developing under control and heat stress conditions at 4 and 10 DAF.

743



745 **Figure S3.** Percent change in A_{leaf} and $A_{panicle}$ at 10 DAF under HS as compared to respective control
 746 values in TEJ-1 and TEJ-2. Error bars represent \pm SE.



748 **Figure S4.** Quantification of single grain weight (mg), spikelet fertility (%), grain length (mm),
749 and grain width (mm) from marked seeds evaluated at the time of physiological maturity.

750

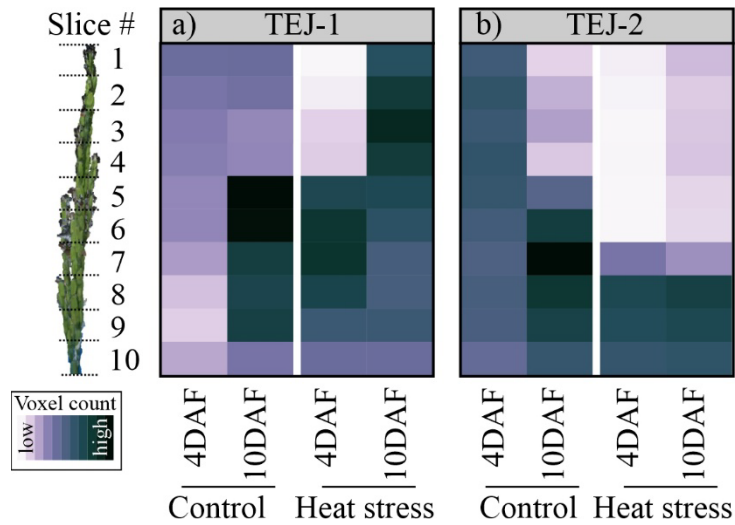
751

752

753

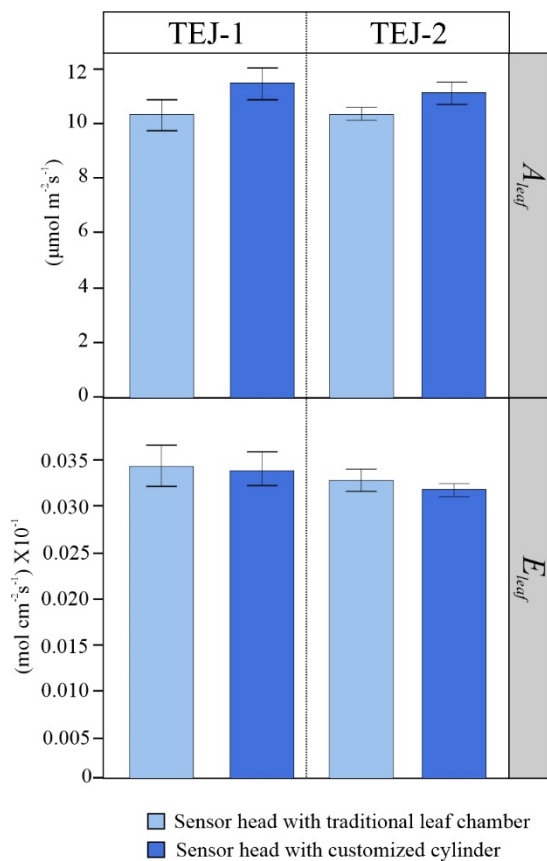
754

755

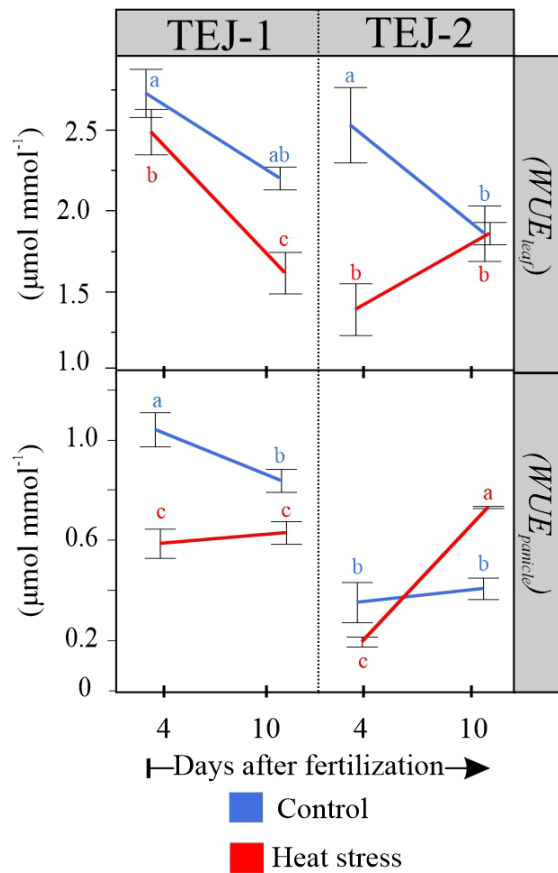


757 **Figure S5.** Shift in voxel count resolved into 3D slices using the panicle point cloud (a) TEJ-1 and (b)
 758 TEJ-2.

759



761 **Figure S6.** Measurements of A_{leaf} and E_{leaf} from randomly selected young green leaf (not flag
 762 leaf) of TEJ-1 and TEJ-2 plants using sensor head equipped with traditional leaf chamber (light
 763 blue) and customized cylinder (dark blue) under control temperature conditions.



765 **Figure S7.** Water use efficiency measurements for leaf (WUE_{leaf}) and panicle ($WUE_{panicle}$) under
766 control and HS for TEJ-1 and TEJ-2.